

Lift and Relax for PDE-constrained inverse problems in seismic imaging

Zhilong Fang^{1,2}, Laurent Demanet^{1,2}

¹Department of Mathematics, Massachusetts Institute of Technology

²Earth Resource Laboratory, Massachusetts Institute of Technology

Abstract

We present Lift and Relax for Waveform Inversion (LRWI), an approach that mitigates the local minima issue in seismic full waveform inversion (FWI) via a combination of two convexification techniques. The first technique (Lift) extends the set of variables in the optimization problem to products of those variables, arranged as a moment matrix. This algebraic idea is a celebrated way to replace a hard polynomial optimization problem by a semidefinite programming approximation. Concretely, both the model and the wavefield are lifted from vectors to rank-2 matrices. The second technique (Relax) invites to consider the wave equation, not as a hard constraint, but as a soft constraint to be satisfied only approximately – a technique known as wavefield reconstruction inversion (WRI). WRI weakens wave-equation constraints by introducing wave-equation misfits as a weighted penalty term in the objective function. The relaxed penalty formulation enables balancing the data and wave-equation misfits by tuning a penalty parameter. Together, “Lift” and “Relax” help reformulate the inverse problem as a set of constraints on a rank-2 moment matrix in a higher dimensional space. Such a lifting strategy permits a good data and wave-equation fit throughout the inversion process, while leaving the numerical rank of the rank-2 moment matrix to be minimized down to one. Numerical examples indicate that compared to FWI and WRI, LRWI can conduct successful inversions using an initial model that would be considered too poor, and data with a starting frequency that would be considered too high, for either method in isolation. Specifically, LRWI increases the acceptable starting frequency from 1.0 Hz and 0.5 Hz to 2.0 Hz and 2.5 for the Marmousi model and the Overthrust model, respectively, in the cases of a linear gradient starting model.

Key words.

Inverse problem, full waveform inversion, lift, relax, PDE

AMS subject classification.

86A22, 35R30

Introduction

Seismic imaging is the primary means for Earth scientists and geophysicists to explore and study Earth’s deep interior, where direct observations are infeasible. Its applications range from studies of Earth’s core, thousands of kilometers below the surface, to detailed images of shallow crustal structures for locating petroleum deposits. During the last thirty years, with the advancements in high-performance computing and the development of wide-aperture and dense data acquisition, seismic imaging techniques have been upgraded from simple and low-resolution ray-based methods to complicated and high-resolution wave-equation-based methods. Especially, during the last two decades, full waveform inversion (FWI) [Tarantola and Valette, 1982, Pratt, 1999, Virieux and Operto, 2009] has become one of the most important approaches because of its potential capability in creating high-resolution subsurface images through the usage of all kinds of waves in the data.

Conventional FWI seeks a subsurface velocity model that can minimize the difference between its predicted data and the observed data in a least-squares sense. A well-known problem associated with conventional FWI is that it suffers from local minima in the objective function caused by the so-called “cycle-skipping” issues. More specifically, if the initial model does not generate predicted data within half a wavelength of the observed data, iterative optimization approaches may stagnate at physically meaningless solutions with a high probability. In order to conduct a successful inversion, conventional FWI needs a good initial model that is kinematically accurate at the longest data wavelengths and data containing enough low frequencies and long offsets [Virieux and Operto, 2009, Vigh et al., 2009, Warner et al., 2013]. Research aimed at mitigating the “cycle-skipping” issue mainly focuses on different misfit functions [Cara and Lévêque, 1987, van Leeuwen and Mulder, 2010, Wu et al., 2013, Engquist and Froese, 2014, Warner and Guasch, 2016, Yang et al., 2018], expanding the search space [van Leeuwen and Herrmann, 2015, Huang et al., 2017, Fang et al., 2018b,a], and the integration with the advanced approach of migration velocity analysis [Symes, 2008, Li et al., 2014].

We propose a two-pronged Lift and Relax waveform inversion (LRWI) approach to mitigating the local minima problem in this paper. The proposed approach consists of two relaxation strategies that expand the search space. The “Relax” strategy is based on the so-called approach wavefield reconstruction inversion (WRI) [van Leeuwen and Herrmann, 2015, Fang et al., 2018b]. WRI first introduces wavefields as additional unknown variables, and then weakens the partial differential equation (PDE) constraints used in conventional FWI by treating the PDE misfit as a weighted penalty term in the objective function. Through tuning the penalty parameter, the resulting approach does not enforce the PDE constraints at each iteration and arguably yields a less non-linear problem in the model parameter. The “Lift” strategy follows the early work in Cosse et al. [2015] that borrows ideas from recent developments in the semidefinite relaxation for polynomial equations to mitigate non-convexity [Lasserre, 2001, Laurent, 2009]. We lift both unknown wavefields and model parameters from 1D vectors to rank-2 matrices, and reformulate the WRI problem as a set of constraints on a rank-2 moment matrix in a higher dimensional space. Such a lifting strategy permits a good data and wave-equation fit throughout the inversion process, while leaving the numerical rank of the moment matrix to be the quantity to minimize – so that this matrix aims to be a rank one matrix at convergence eventually.

Compared to conventional FWI, the proposed LRWI approach has three major advantages. First, the computation of the gradients does not require adjoint or reverse-time wavefields. Secondly, the “Relax” and “Lift” strategies enable us to fit both data misfit and PDE misfit even with poor models. Thirdly, the rank-2 formulation provides us with the potential to utilize information from the two components in the rank-2 model matrix simultaneously. The last two properties, in conjunction with the expanded search space, may result in an optimization formulation that is less prone to local minima. We present numerical examples on both Marmousi and Overthrust models to illustrate the feasibility and advantages of the proposed approach.

The paper is organized as follows. First, we review the basic conception and formulation of conventional FWI. Next, we derive the formulation for the proposed rank-2 LRWI. Then, we derive all the necessary components for the efficient optimization strategy in detail. Finally, we present numerical examples on Marmousi and

Overthrust models to illustrate the feasibility and advantages of LRWI and conclude the paper with a detailed discussion.

Methodology

Given a seismic data set $\mathbf{d} \in \mathbb{R}^{n_s \times n_r \times n_f}$ with n_s sources, n_r receivers, and n_f frequencies, FWI aims to reconstruct the discretized n_g -dimensional squared slowness model \mathbf{m} from \mathbf{d} by solving the following PDE-constrained optimization problem:

$$\begin{aligned} \min_{\mathbf{m}, \mathbf{u}} f_f(\mathbf{m}, \mathbf{u}) &= \frac{1}{2} \sum_{i,j}^{n_s, n_f} \|\mathbf{P}\mathbf{u}_{i,j} - \mathbf{d}_{i,j}\|_2^2, \\ \text{subject to } (\Delta + \omega_j^2 \mathbf{m})\mathbf{u}_{i,j} &= \mathbf{q}_{i,j}, \end{aligned} \quad (1)$$

where the operator \mathbf{P} projects the wavefield $\mathbf{u}_{i,j}$ corresponding to the i^{th} source $\mathbf{q}_{i,j}$ with frequency ω_j onto the receiver locations. The operator Δ represents the Laplacian operator, and the equation $(\Delta + \omega_j^2 \mathbf{m})\mathbf{u}_{i,j} = \mathbf{q}_{i,j}$ is known as the Helmholtz equation.

The optimization problem in Equation 1 requires a solution in $\mathbb{R}^{n_g} \times \mathbb{C}^{n_u}$ with $n_u = n_s \times n_r \times n_g$, which is infeasible for most practical applications because we cannot afford to store all the unknown variables. To reduce the dimensionality of the search space, the conventional adjoint-state method [Virieux and Operto, 2009] eliminates the PDE constraint $(\Delta + \omega_j^2 \mathbf{m})\mathbf{u}_{i,j} = \mathbf{q}_{i,j}$ through solving the PDE straightforwardly, yielding the following reduced problem:

$$\begin{aligned} \min_{\mathbf{m}} f_r(\mathbf{m}) &= \frac{1}{2} \sum_{i,j}^{n_s, n_f} \|\mathbf{P}\mathbf{A}_j(\mathbf{m})^{-1}\mathbf{q}_{i,j} - \mathbf{d}_{i,j}\|_2^2, \\ \text{with } \mathbf{A}_j(\mathbf{m}) &= \Delta + \omega_j^2 \mathbf{m}, \end{aligned} \quad (2)$$

whose search space is \mathbb{R}^{n_g} . Although the dimensionality of the search space reduces from $n_u + n_g$ to n_g , the trade-off lies in the fact that the inversion of the Helmholtz matrix introduces a very strong nonlinearity into the problem, yielding an objective function $f_r(\mathbf{m})$ with many local minima.

WRI with a rank- r relaxation

In this work, we aim to mitigate the local minima issue of conventional FWI by proposing a Lift and Relax formulation in the rank- r case. To simplify the notation, we will omit the dependence of the variables on the source and frequency indexes i and j from now on.

We first follow van Leeuwen and Herrmann [2015] and relax the PDE constraint in Equation 1 by considering the PDE misfit as a weighted penalty term as follows:

$$\min_{\mathbf{m}, \mathbf{u}} f_p(\mathbf{m}, \mathbf{u}) = \frac{1}{2} \|\mathbf{P}\mathbf{u} - \mathbf{d}\|_2^2 + \frac{\lambda}{2} \|(\Delta + \omega^2 \mathbf{m})\mathbf{u} - \mathbf{q}\|_2^2. \quad (3)$$

The penalty parameter λ enables us to balance the PDE and data misfits and provides the freedom to design a search path in the enlarged space that can potentially bypass the local minima in the objective function of conventional FWI.

Following the PDE relaxation, we introduce an additional rank- r relaxation to expand the search space into a higher dimension space, which is motivated from the following matrix expression of the unknown parameters

\mathbf{m} and \mathbf{u} :

$$\mathbf{X} = \begin{bmatrix} \mathbf{X}_{11} & \mathbf{X}_{12} & \mathbf{X}_{13} \\ \mathbf{X}_{21} & \mathbf{X}_{22} & \mathbf{X}_{23} \\ \mathbf{X}_{31} & \mathbf{X}_{32} & \mathbf{X}_{33} \end{bmatrix} = [\mathbf{1}, \mathbf{m}^\top, \mathbf{u}^\top]^\top [\mathbf{1}, \mathbf{m}^\top, \mathbf{u}^\top]. \quad (4)$$

Clearly, the matrix \mathbf{X} is a rank-1 positive semidefinite matrix. Based on Equation 4, we can lift the original WRI problem from optimizing over vectors \mathbf{m} and \mathbf{u} to optimizing over the matrix \mathbf{X} . In the course of doing so, the direct correspondence to \mathbf{m} and \mathbf{u} in Equation 4 is not directly imposed, but the objective in Equation 3 is rewritten with the blocks of \mathbf{X} serving as proxies for \mathbf{m} , \mathbf{u} , and the product $\mathbf{m}\mathbf{u}^\top$. This yields the following equivalent optimization problem:

$$\begin{aligned} \min_{\mathbf{X}} f_{\text{px}}(\mathbf{X}) &= \frac{1}{2} \|\mathbf{P}\mathbf{X}_{31} - \mathbf{d}\|_2^2 + \frac{\lambda}{2} \|\Delta\mathbf{X}_{31} + \omega^2 \text{diag}(\mathbf{X}_{32}) - \mathbf{q}\|_2^2, \\ \text{subject to } & \mathbf{X}_{11} = 1, \\ & \mathbf{X} \succeq 0, \\ & \text{rank}(\mathbf{X}) = 1. \end{aligned} \quad (5)$$

The ‘‘Lift’’ relaxation then consists in dropping the rank-1 constraint.

The new objective function $f_{\text{px}}(\mathbf{X})$ is a quadratic function with respect to the matrix \mathbf{X} , which is much simpler than the original FWI and WRI objective functions. Since $\mathbf{X} \in \mathbb{C}^{(n_u+n_g+1)^2}$, we are not able to optimize over \mathbf{X} directly for large-scale realistic applications. Nonetheless, as stated by Cosse et al. [2015], it is possible for us to obtain a computationally feasible formulation with a reasonable storage requirement by introducing a rank- r factorization $\mathbf{R}\mathbf{R}^\top$ for the matrix \mathbf{X} :

$$\begin{aligned} \min_{\mathbf{R}} f_{\text{pr}}(\mathbf{R}) &= \frac{1}{2} \|\mathbf{P}(\mathbf{R}_3\mathbf{R}_1^\top) - \mathbf{d}\|_2^2 + \frac{\lambda}{2} \|\Delta(\mathbf{R}_3\mathbf{R}_1^\top) + \omega^2 \text{diag}(\mathbf{R}_3\mathbf{R}_2^\top) - \mathbf{q}\|_2^2, \\ \text{subject to } & \mathbf{R}_1\mathbf{R}_1^\top = 1, \end{aligned} \quad (6)$$

where $\mathbf{R} = (\mathbf{R}_1^\top, \mathbf{R}_2^\top, \mathbf{R}_3^\top)^\top$ with $\mathbf{R}_1 = [\alpha_1, \dots, \alpha_r] \in \mathbb{R}^{1 \times r}$, $\mathbf{R}_2 = [\tilde{\mathbf{m}}_1, \dots, \tilde{\mathbf{m}}_r] \in \mathbb{R}^{n_g \times r}$, and $\mathbf{R}_3 = [\tilde{\mathbf{u}}^1, \dots, \tilde{\mathbf{u}}^r] \in \mathbb{C}^{n_u \times r}$. This block representation of \mathbf{R} leads to a representation of \mathbf{X} as a sum of rank-1 matrices,

$$\mathbf{X} \approx \mathbf{R}\mathbf{R}^\top = \sum_{l=1}^r \begin{bmatrix} \alpha_l^2 & \alpha_l \tilde{\mathbf{m}}_l^\top & \alpha_l \tilde{\mathbf{u}}_l^\top \\ \alpha_l \tilde{\mathbf{m}}_l & \tilde{\mathbf{m}}_l \tilde{\mathbf{m}}_l^\top & \tilde{\mathbf{m}}_l \tilde{\mathbf{u}}_l^\top \\ \alpha_l \tilde{\mathbf{u}}_l & \tilde{\mathbf{u}}_l \tilde{\mathbf{m}}_l^\top & \tilde{\mathbf{u}}_l \tilde{\mathbf{u}}_l^\top \end{bmatrix}. \quad (7)$$

When $r = 1$, the optimization problem in Equation 6 will reduce to the original WRI problem in Equation 3. A larger r yields a stronger relaxation but introduces more computational cost and storage requirements.

rank-2 relaxation

In this work, we present a rank-2 formulation for the optimization problem in Equation 6 to balance the relaxation and computational costs. When selecting $r = 2$, we have

$$\begin{aligned} \mathbf{m} &= \alpha_1 \tilde{\mathbf{m}}_1 + \alpha_2 \tilde{\mathbf{m}}_2, \\ \mathbf{u} &= \alpha_1 \tilde{\mathbf{u}}_1 + \alpha_2 \tilde{\mathbf{u}}_2, \\ \mathbf{m} \odot \mathbf{u} &= \tilde{\mathbf{m}}_1 \odot \tilde{\mathbf{u}}_1 + \tilde{\mathbf{m}}_2 \odot \tilde{\mathbf{u}}_2, \\ 1 &= \alpha_1^2 + \alpha_2^2, \end{aligned} \quad (8)$$

where the operator \odot represents the pointwise multiplication or the Hadamard product. The rank-2 expression in Equation 8 yields the following optimization problem:

$$\min_{\tilde{\mathbf{m}}, \tilde{\mathbf{u}}, \alpha} f_{\text{p}_2}(\tilde{\mathbf{m}}, \tilde{\mathbf{u}}, \alpha) = \frac{1}{2} \left\| \sum_{l=1}^2 \mathbf{P} \alpha_l \tilde{\mathbf{u}}_l - \mathbf{d} \right\|_2^2 + \frac{\lambda}{2} \left\| \sum_{l=1}^2 \alpha_l \Delta \tilde{\mathbf{u}}_l + \omega^2 \sum_{l=1}^2 \tilde{\mathbf{m}}_l \odot \tilde{\mathbf{u}}_l - \mathbf{q} \right\|_2^2. \quad (9)$$

It is easy to verify that this optimization problem has infinite solutions. Indeed, for any fixed pair of $(\tilde{\mathbf{m}}^*, \tilde{\mathbf{u}}^*)$, the optimal $\tilde{\mathbf{u}}^*$ for the objective function $f_{p_2}(\tilde{\mathbf{m}}^*, \tilde{\mathbf{u}}, \alpha^*)$ should satisfy the following equation:

$$\mathbf{S}\tilde{\mathbf{u}}^* = \begin{bmatrix} \alpha_1 \mathbf{P}, & \alpha_2 \mathbf{P} \\ \lambda^{\frac{1}{2}}(\alpha_1 \Delta + \omega^2 \tilde{\mathbf{m}}_1) & \lambda^{\frac{1}{2}}(\alpha_2 \Delta + \omega^2 \tilde{\mathbf{m}}_2) \end{bmatrix} \begin{bmatrix} \tilde{\mathbf{u}}_1^* \\ \tilde{\mathbf{u}}_2^* \end{bmatrix} = \begin{bmatrix} \mathbf{d} \\ \lambda^{\frac{1}{2}} \mathbf{q} \end{bmatrix}. \quad (10)$$

Since the matrix \mathbf{S} is an underdetermined $(n_g+n_r) \times 2n_g$ matrix with $n_g > n_r$, the linear Equation 10 has infinite solutions for $\tilde{\mathbf{u}}^*$. As a result, there are infinite global minima $(\tilde{\mathbf{m}}^*, \tilde{\mathbf{u}}^*, \alpha^*)$ s satisfying $f_{p_2}(\tilde{\mathbf{m}}^*, \tilde{\mathbf{u}}^*, \alpha^*) = 0$.

To mitigate the nonuniqueness issue of optimizing Equation 9, we need additional information to regularize the problem. We notice that the original lifted problem in Equation 5 has the constraint of $\text{rank}(\mathbf{X}) = 1$, which is not involved in the rank-2 formulation. Therefore, to derive our regularization, we reimpose this information. We do not straightforwardly require $\text{rank}(\mathbf{R}) = 1$, otherwise it will downgrade the problem to the rank-1 case, which is the original WRI problem. Instead, we use another necessary condition for a rank-1 matrix to introduce a weaker regularization. If the matrix \mathbf{R} is a rank-1 matrix, then its three components $\mathbf{R}_1 = [\alpha_1, \alpha_2]$, $\mathbf{R}_2 = [\tilde{\mathbf{m}}_1, \tilde{\mathbf{m}}_2]$ and $\mathbf{R}_3 = [\tilde{\mathbf{u}}_1, \tilde{\mathbf{u}}_2]$ should satisfy the following requirements:

$$\begin{aligned} \alpha_1 \tilde{\mathbf{m}}_2 &= \alpha_2 \tilde{\mathbf{m}}_1, \\ \alpha_1 \tilde{\mathbf{u}}_2 &= \alpha_2 \tilde{\mathbf{u}}_1, \\ \tilde{\mathbf{m}}_1 \odot \tilde{\mathbf{u}}_2 &= \tilde{\mathbf{m}}_2 \odot \tilde{\mathbf{u}}_1. \end{aligned} \quad (11)$$

We can use these properties to regularize the problem. In this work, since we are more interested in $\tilde{\mathbf{m}}$ and $\tilde{\mathbf{u}}$ than α , we use the third property to introduce an additional regularization to the optimization problem in Equation 9 as follows:

$$\begin{aligned} \min_{\tilde{\mathbf{m}}, \tilde{\mathbf{u}}, \alpha} f_{p_2}(\tilde{\mathbf{m}}, \tilde{\mathbf{u}}, \alpha) &= \frac{1}{2} \left\| \sum_{l=1}^2 \mathbf{P} \alpha_l \tilde{\mathbf{u}}_l - \mathbf{d} \right\|_2^2 \\ &+ \frac{\lambda}{2} \left\| \sum_{l=1}^2 \alpha_l \Delta \tilde{\mathbf{u}}_l + \omega^2 \sum_{l=1}^2 \tilde{\mathbf{m}}_l \odot \tilde{\mathbf{u}}_l - \mathbf{q} \right\|_2^2 \\ &+ \frac{\gamma}{2} \left\| \tilde{\mathbf{m}}_1 \odot \tilde{\mathbf{u}}_2 - \tilde{\mathbf{m}}_2 \odot \tilde{\mathbf{u}}_1 \right\|_2^2, \\ \text{subject to } &\alpha_1^2 + \alpha_2^2 = 1, \end{aligned} \quad (12)$$

where the penalty parameter γ controls the strength of the rank-1 regularization.

Finally, we can simplify the constrained optimization problem in Equation 9 to an unconstrained problem by eliminating the constraint $\alpha_1^2 + \alpha_2^2 = 1$ with a simple polar coordinates transform:

$$\alpha_1 = \sin \theta \quad \text{and} \quad \alpha_2 = \cos \theta, \quad (13)$$

yielding the following unconstrained optimization problem:

$$\begin{aligned} \min_{\tilde{\mathbf{m}}, \tilde{\mathbf{u}}, \theta} f_{p_2}(\tilde{\mathbf{m}}, \tilde{\mathbf{u}}, \theta) &= \frac{1}{2} \left\| \mathbf{P}(\sin \theta \tilde{\mathbf{u}}_1 + \cos \theta \tilde{\mathbf{u}}_2) - \mathbf{d} \right\|_2^2 \\ &+ \frac{\lambda}{2} \left\| \Delta(\sin \theta \tilde{\mathbf{u}}_1 + \cos \theta \tilde{\mathbf{u}}_2) + \omega^2 \sum_{l=1}^2 \tilde{\mathbf{m}}_l \odot \tilde{\mathbf{u}}_l - \mathbf{q} \right\|_2^2 \\ &+ \frac{\gamma}{2} \left\| \tilde{\mathbf{m}}_1 \odot \tilde{\mathbf{u}}_2 - \tilde{\mathbf{m}}_2 \odot \tilde{\mathbf{u}}_1 \right\|_2^2. \end{aligned} \quad (14)$$

Variable projection and optimization scheme

The optimization problem in Equation 14 still faces the challenge of a large storage requirement. In order to reduce the storage requirement, we use the variable projection method [Golub and Pereyra, 2003] to project out the wavefields $\tilde{\mathbf{u}}$, which is the main source of the storage cost. For any pair of $(\tilde{\mathbf{m}}^*, \theta^*)$, the objective function $f_{p_2}(\tilde{\mathbf{m}}^*, \tilde{\mathbf{u}}, \theta^*)$ is quadratic with respect to $\tilde{\mathbf{u}}$, whose minimizer has an analytical solution:

$$\tilde{\mathbf{u}}^* = (\tilde{\mathbf{S}}^\top \tilde{\mathbf{S}})^{-1} \tilde{\mathbf{S}}^\top \begin{bmatrix} \mathbf{d} \\ \lambda^{\frac{1}{2}} \mathbf{q} \\ 0 \end{bmatrix}, \quad (15)$$

with

$$\tilde{\mathbf{S}} = \begin{bmatrix} \sin \theta \mathbf{P} & \cos \theta \mathbf{P} \\ \lambda^{\frac{1}{2}} \tilde{\mathbf{A}}(\tilde{\mathbf{m}}_1) & \lambda^{\frac{1}{2}} \tilde{\mathbf{A}}(\tilde{\mathbf{m}}_2) \\ \gamma^{\frac{1}{2}} \text{diag}(\tilde{\mathbf{m}}_2) & -\gamma^{\frac{1}{2}} \text{diag}(\tilde{\mathbf{m}}_1) \end{bmatrix}, \quad (16)$$

$$\text{with } \tilde{\mathbf{A}}(\tilde{\mathbf{m}}_1) = \sin \theta \Delta + \omega^2 \tilde{\mathbf{m}}_1, \quad \text{and } \tilde{\mathbf{A}}(\tilde{\mathbf{m}}_2) = \cos \theta \Delta + \omega^2 \tilde{\mathbf{m}}_2.$$

Replacing the variable $\tilde{\mathbf{u}}$ in Equation 14 by the optimal solution $\tilde{\mathbf{u}}^*(\tilde{\mathbf{m}}, \theta)$, we obtain a reduced objective function $\bar{f}_{p_2}(\tilde{\mathbf{m}}, \theta) = f_{p_2}(\tilde{\mathbf{m}}, \tilde{\mathbf{u}}^*(\tilde{\mathbf{m}}, \theta), \theta)$. We can use the chain rule to compute the derivatives of $\nabla_{\tilde{\mathbf{m}}} \bar{f}_{p_2}(\tilde{\mathbf{m}}, \theta)$ and $\nabla_{\theta} \bar{f}_{p_2}(\tilde{\mathbf{m}}, \theta)$ as follows:

$$\begin{aligned} \nabla_{\tilde{\mathbf{m}}} \bar{f}_{p_2}(\tilde{\mathbf{m}}, \theta) &= \nabla_{\tilde{\mathbf{m}}} f_{p_2}(\tilde{\mathbf{m}}, \tilde{\mathbf{u}}^*(\tilde{\mathbf{m}}, \theta), \theta) \\ &= \nabla_{\tilde{\mathbf{m}}} f_{p_2}(\tilde{\mathbf{m}}, \tilde{\mathbf{u}}, \alpha)|_{\tilde{\mathbf{u}}=\tilde{\mathbf{u}}^*} + \nabla_{\tilde{\mathbf{u}}} f_{p_2}(\tilde{\mathbf{m}}, \tilde{\mathbf{u}}, \alpha)|_{\tilde{\mathbf{u}}=\tilde{\mathbf{u}}^*} \nabla_{\tilde{\mathbf{m}}} \tilde{\mathbf{u}}, \\ \nabla_{\theta} \bar{f}_{p_2}(\tilde{\mathbf{m}}, \theta) &= \nabla_{\theta} f_{p_2}(\tilde{\mathbf{m}}, \tilde{\mathbf{u}}^*(\tilde{\mathbf{m}}, \theta), \theta) \\ &= \nabla_{\theta} f_{p_2}(\tilde{\mathbf{m}}, \tilde{\mathbf{u}}, \alpha)|_{\tilde{\mathbf{u}}=\tilde{\mathbf{u}}^*} + \nabla_{\tilde{\mathbf{u}}} f_{p_2}(\tilde{\mathbf{m}}, \tilde{\mathbf{u}}, \alpha)|_{\tilde{\mathbf{u}}=\tilde{\mathbf{u}}^*} \nabla_{\theta} \tilde{\mathbf{u}}. \end{aligned} \quad (17)$$

The most important property of the variable projection method lies in the fact that $\tilde{\mathbf{u}}^*$ minimizes the objective function $f_{p_2}(\tilde{\mathbf{m}}, \tilde{\mathbf{u}}, \alpha)$ for fixed $(\tilde{\mathbf{m}}, \theta)$, satisfying the condition $\nabla_{\tilde{\mathbf{u}}} f_{p_2}(\tilde{\mathbf{m}}, \tilde{\mathbf{u}}, \alpha)|_{\tilde{\mathbf{u}}=\tilde{\mathbf{u}}^*} = 0$. Therefore, we can drop out the complicated terms $\nabla_{\tilde{\mathbf{u}}} f_{p_2}(\tilde{\mathbf{m}}, \tilde{\mathbf{u}}, \alpha)|_{\tilde{\mathbf{u}}=\tilde{\mathbf{u}}^*} \nabla_{\tilde{\mathbf{m}}} \tilde{\mathbf{u}}$ and $\nabla_{\tilde{\mathbf{u}}} f_{p_2}(\tilde{\mathbf{m}}, \tilde{\mathbf{u}}, \alpha)|_{\tilde{\mathbf{u}}=\tilde{\mathbf{u}}^*} \nabla_{\theta} \tilde{\mathbf{u}}$ in the expressions of $\nabla_{\tilde{\mathbf{m}}} \bar{f}_{p_2}(\tilde{\mathbf{m}}, \theta)$ and $\nabla_{\theta} \bar{f}_{p_2}(\tilde{\mathbf{m}}, \theta)$, and simplify them as follows:

$$\begin{aligned} \nabla_{\tilde{\mathbf{m}}} \bar{f}_{p_2}(\tilde{\mathbf{m}}, \theta) &= \nabla_{\tilde{\mathbf{m}}} f_{p_2}(\tilde{\mathbf{m}}, \tilde{\mathbf{u}}, \alpha)|_{\tilde{\mathbf{u}}=\tilde{\mathbf{u}}^*}, \\ \nabla_{\theta} \bar{f}_{p_2}(\tilde{\mathbf{m}}, \theta) &= \nabla_{\theta} f_{p_2}(\tilde{\mathbf{m}}, \tilde{\mathbf{u}}, \alpha)|_{\tilde{\mathbf{u}}=\tilde{\mathbf{u}}^*}. \end{aligned} \quad (18)$$

Following Equation 18, the expressions for $\nabla_{\tilde{\mathbf{m}}} \bar{f}_{p_2}(\tilde{\mathbf{m}}, \theta)$ and $\nabla_{\theta} \bar{f}_{p_2}(\tilde{\mathbf{m}}, \theta)$ can be derived as follows:

$$\begin{aligned} \nabla_{\tilde{\mathbf{m}}} \bar{f}_{p_2}(\tilde{\mathbf{m}}, \theta) &= \begin{bmatrix} \nabla_{\tilde{\mathbf{m}}_1} \bar{f}_{p_2}(\tilde{\mathbf{m}}, \theta) \\ \nabla_{\tilde{\mathbf{m}}_2} \bar{f}_{p_2}(\tilde{\mathbf{m}}, \theta) \end{bmatrix} \\ &= \begin{bmatrix} \lambda(\omega^2 \text{diag}(\tilde{\mathbf{u}}_1^*))^\top \mathbf{p} + \gamma(\text{diag}(\tilde{\mathbf{u}}_2^*))^\top \mathbf{s} \\ \lambda(\omega^2 \text{diag}(\tilde{\mathbf{u}}_2^*))^\top \mathbf{p} - \gamma(\text{diag}(\tilde{\mathbf{u}}_1^*))^\top \mathbf{s} \end{bmatrix}, \\ \nabla_{\theta} \bar{f}_{p_2}(\tilde{\mathbf{m}}, \theta) &= \cos \theta [(\mathbf{P} \tilde{\mathbf{u}}_1^*)^\top \mathbf{r} + \lambda(\Delta \tilde{\mathbf{u}}_1^*)^\top \mathbf{p}] \\ &\quad - \sin \theta [(\mathbf{P} \tilde{\mathbf{u}}_2^*)^\top \mathbf{r} + \lambda(\Delta \tilde{\mathbf{u}}_2^*)^\top \mathbf{p}], \end{aligned} \quad (19)$$

where

$$\begin{aligned} \mathbf{p} &= \Delta(\sin \theta \tilde{\mathbf{u}}_1^* + \cos \theta \tilde{\mathbf{u}}_2^*) + \omega^2 \sum_{l=1}^2 \tilde{\mathbf{m}}_l \odot \tilde{\mathbf{u}}_l^* - \mathbf{q}, \\ \mathbf{s} &= \tilde{\mathbf{m}}_1 \odot \tilde{\mathbf{u}}_2^* - \tilde{\mathbf{m}}_2 \odot \tilde{\mathbf{u}}_1^*, \\ \mathbf{r} &= \mathbf{P}(\sin \theta \tilde{\mathbf{u}}_1^* + \cos \theta \tilde{\mathbf{u}}_2^*) - \mathbf{d}. \end{aligned} \quad (20)$$

Once obtained $\tilde{\mathbf{u}}^*$, Equations 19 and 20 imply that the computation of the gradients $\nabla_{\tilde{\mathbf{m}}}\bar{f}_{p_2}(\tilde{\mathbf{m}},\theta)$ and $\nabla_{\theta}\bar{f}_{p_2}(\tilde{\mathbf{m}},\theta)$ only involves simple and cheap matrix-vector multiplications and does not involve any additional computationally intensive matrix inverses. Compared to the conventional adjoint-state method that requires to invert an additional adjoint Helmholtz matrix to obtain the gradient, the proposed method reduces computational cost for computing the gradient.

With the derivatives in Equation 19, we can use optimization algorithms like gradient descent and limited-memory Broyden-Fletcher-Goldfarb-Shanno (l-BFGS) method [Nocedal and Wright, 2006] that only needs the gradient information to solve the optimization problem. During the optimization, since $\tilde{\mathbf{m}}$ and θ are very different in scale and have very different sensitivities to the objective function, we propose to update them alternately. During each iteration, we first conduct an l-BFGS update on $\tilde{\mathbf{m}}$, then we use a gradient descent step to update θ . Algorithm 1 illustrates the pseudo code of the two-stage l-BFGS method.

Algorithm 1 Rank-2 LRWI

1. Initialization with $\tilde{\mathbf{m}}_1^{(0)}$, $\tilde{\mathbf{m}}_2^{(0)}$ and $\theta^{(0)}$
 2. **for** $k = 1 \rightarrow n_{it}$
 3. Compute $\tilde{\mathbf{u}}^{*(k)}$ by Equation 15
 4. Compute $\bar{f}_{p_2}^{(k)}(\tilde{\mathbf{m}}^{(k)},\theta^{(k)})$ and $\nabla_{\tilde{\mathbf{m}}}\bar{f}_{p_2}^{(k)}(\tilde{\mathbf{m}}^{(k)},\theta^{(k)})$ by Equations 19
 5. l-BFGS step in $\tilde{\mathbf{m}}^{(k)}$ to get $\tilde{\mathbf{m}}^{(k+1)}$
 6. Compute $\nabla_{\theta}\bar{f}_{p_2}^{(k)}(\tilde{\mathbf{m}}^{(k+1)},\theta^{(k)})$ by Equations 19
 7. Gradient descent step in $\theta^{(k)}$ to get $\theta^{(k+1)}$
 8. **end**
 9. Obtain θ^* and $\tilde{\mathbf{m}}^* = (\tilde{\mathbf{m}}_1^*, \tilde{\mathbf{m}}_2^*)$
 10. Output $\mathbf{m}^* = \sin\theta^*\tilde{\mathbf{m}}_1^* + \cos\theta^*\tilde{\mathbf{m}}_2^*$
-

Selection of λ and γ

The selection of λ and γ plays an important role in the proposed LRWI, because λ and γ affect the condition number of the matrix $\tilde{\mathbf{S}}$ in Equation 15 and the search path. An appropriate selection can produce a search path that bypasses the local minima of conventional FWI and also speeds up the optimization procedure. In this work, we propose a two-stage unit-free strategy to select λ and γ .

We first determine the selection of λ . van Leeuwen and Herrmann [2015] and Fang et al. [2018a] studied the selection of λ for WRI and proposed a natural scaling for λ , i.e. $\lambda > \mu_1(\mathbf{A}^{-\top}\mathbf{P}^{\top}\mathbf{P}\mathbf{A}^{-1})$ can be considered large, while $\lambda < \mu_1(\mathbf{A}^{-\top}\mathbf{P}^{\top}\mathbf{P}\mathbf{A}^{-1})$ can be considered small, where the matrix \mathbf{A} denotes the Helmholtz matrix parameterized by the current model \mathbf{m} and $\mu_1(\mathbf{A}^{-\top}\mathbf{P}^{\top}\mathbf{P}\mathbf{A}^{-1})$ denotes the largest eigenvalue of the matrix $\mathbf{A}^{-\top}\mathbf{P}^{\top}\mathbf{P}\mathbf{A}^{-1}$. Specifically, when $\lambda < 10^{-2}\mu_1(\mathbf{A}^{-\top}\mathbf{P}^{\top}\mathbf{P}\mathbf{A}^{-1})$, the simulated wavefields tend to fit the observed data while leaving a big misfit for the PDE; when $\lambda > 10^2\mu_1(\mathbf{A}^{-\top}\mathbf{P}^{\top}\mathbf{P}\mathbf{A}^{-1})$, the opposite holds. In practice, considering the large computational cost of calculating μ_1 , van Leeuwen and Herrmann [2015] suggest using μ_1 parameterized with the initial model $\mathbf{m}^{(0)}$ to select the penalty parameter λ . Following van Leeuwen and Herrmann [2015] and Fang et al. [2018a], we select λ according to the value $\mu_1(\mathbf{A}(\mathbf{m}^{(0)})^{-\top}\mathbf{P}^{\top}\mathbf{P}\mathbf{A}(\mathbf{m}^{(0)})^{-1})$, where $\mathbf{m}^{(0)} = \sin\theta^{(0)}\tilde{\mathbf{m}}^{(0)} + \cos\theta^{(0)}\tilde{\mathbf{m}}^{(0)}$.

With λ in hand, the selection of γ will determine the condition number of the matrix $\tilde{\mathbf{S}}$. Since both blocks $\begin{bmatrix} \sin\theta\mathbf{P} & \cos\theta\mathbf{P} \\ \lambda^{\frac{1}{2}}\tilde{\mathbf{A}}(\tilde{\mathbf{m}}_1) & \lambda^{\frac{1}{2}}\tilde{\mathbf{A}}(\tilde{\mathbf{m}}_2) \end{bmatrix}$ and $[\gamma^{\frac{1}{2}}\text{diag}(\tilde{\mathbf{m}}_2) \quad -\gamma^{\frac{1}{2}}\text{diag}(\tilde{\mathbf{m}}_1)]$ are underdetermined, either a very large γ or a very small γ will lead to a bad conditioned matrix $\tilde{\mathbf{S}}$. Indeed the matrix $\tilde{\mathbf{S}}^{\top}\tilde{\mathbf{S}}$ in Equation 15 has the following

expression:

$$\begin{aligned}
\tilde{\mathbf{S}}^\top \tilde{\mathbf{S}} &= \begin{bmatrix} \mathbf{T}_{1,1} & \mathbf{T}_{1,2} \\ \mathbf{T}_{2,1} & \mathbf{T}_{2,2} \end{bmatrix}, \quad \text{with} \\
\mathbf{T}_{1,1} &= \alpha_1^2 \mathbf{P}^\top \mathbf{P} + \lambda \tilde{\mathbf{A}}(\tilde{\mathbf{m}}_1)^\top \tilde{\mathbf{A}}(\tilde{\mathbf{m}}_1) + \gamma \text{diag}(\tilde{\mathbf{m}}_2 \odot \tilde{\mathbf{m}}_2), \\
\mathbf{T}_{1,2} &= \alpha_1 \alpha_2 \mathbf{P}^\top \mathbf{P} + \lambda \tilde{\mathbf{A}}(\tilde{\mathbf{m}}_1)^\top \tilde{\mathbf{A}}(\tilde{\mathbf{m}}_2) - \gamma \text{diag}(\tilde{\mathbf{m}}_1 \odot \tilde{\mathbf{m}}_2), \\
\mathbf{T}_{2,1} &= \alpha_1 \alpha_2 \mathbf{P}^\top \mathbf{P} + \lambda \tilde{\mathbf{A}}(\tilde{\mathbf{m}}_2)^\top \tilde{\mathbf{A}}(\tilde{\mathbf{m}}_1) - \gamma \text{diag}(\tilde{\mathbf{m}}_1 \odot \tilde{\mathbf{m}}_2), \\
\mathbf{T}_{2,2} &= \alpha_2^2 \mathbf{P}^\top \mathbf{P} + \lambda \tilde{\mathbf{A}}(\tilde{\mathbf{m}}_2)^\top \tilde{\mathbf{A}}(\tilde{\mathbf{m}}_2) + \gamma \text{diag}(\tilde{\mathbf{m}}_1 \odot \tilde{\mathbf{m}}_1).
\end{aligned} \tag{21}$$

Equation 21 motivates us to derive the scaling of γ by comparing $\gamma \tilde{\mathbf{m}}_i \odot \tilde{\mathbf{m}}_j$ with the diagonal part of the matrices $\mathbf{T}(\lambda) = \{\mathbf{T}_{i,j} = \lambda \tilde{\mathbf{A}}(\tilde{\mathbf{m}}_i)^\top \tilde{\mathbf{A}}(\tilde{\mathbf{m}}_j) + \alpha_i \alpha_j \mathbf{P}^\top \mathbf{P}\}_{1 \leq i, j \leq 2}$. A natural scaling for γ would be the fraction between the ℓ_2 -norm of the vector $\text{diag}(\mathbf{T}_{i,j})$ and the ℓ_2 -norm of the vector $\tilde{\mathbf{m}}_i \odot \tilde{\mathbf{m}}_j$, i.e., $\frac{\|\text{diag}(\mathbf{T}_{i,j})\|_2}{\|\tilde{\mathbf{m}}_i \odot \tilde{\mathbf{m}}_j\|_2}$. Therefore, γ is large if $\gamma > \mu_2(\mathbf{T}(\lambda)) = \max\{\frac{\|\text{diag}(\mathbf{T}_{i,j})\|_2}{\|\tilde{\mathbf{m}}_i \odot \tilde{\mathbf{m}}_j\|_2}\}_{1 \leq i, j \leq 2}$. γ is small for the opposite case.

In general, at the beginning of the optimization, we can select a small λ and a small γ to relax both the PDE constraint and the rank-1 constraint. As the optimization proceeds, we can increase λ and γ to strengthen both constraints so that the solution can converge to the optimal solution of conventional FWI.

Computational cost analysis

The major computational cost of the proposed LRWI is to invert the $2n_g \times 2n_g$ matrix $\tilde{\mathbf{S}}^\top \tilde{\mathbf{S}}$ in Equation 15 to obtain $\tilde{\mathbf{u}}^*$. If we use a direct solver to invert $\tilde{\mathbf{S}}^\top \tilde{\mathbf{S}}$, the computational cost will be $\mathcal{O}(8n_g^3)$. With $\tilde{\mathbf{u}}^*$ in hand, the computation of the gradients does not include additional matrix inverses. At each iteration, we alternately update $\tilde{\mathbf{m}}$ and θ . Therefore, the total computational cost for LRWI is $\mathcal{O}(16n_g^3 n_f)$ for each iteration. Compared to conventional FWI, whose computational cost is $\mathcal{O}(2n_g^3 n_f)$ for each iteration, LRWI is eight times expensive. Considering the increased computational cost, instead of using LRWI for the whole inversion, we suggest using LRWI to create a better initial model for FWI.

Numerical examples

To investigate the feasibility of the proposed LRWI approach, we conduct numerical examples on two well-known models i.e. the Marmousi model [Versteeg, 1994] and the Overthrust model [Aminzadeh et al., 1996]. In both examples, we will study the performances of the proposed LRWI for different selections of λ and γ , and investigate the performance with respect to the starting frequency.

Marmousi model

We first conduct an example on the Marmousi-2 model \mathbf{m}_t shown in Figure 1a. We use a Ricker wavelet centered at 15Hz to simulate 49 sources at the depth of $z = 0.04\text{km}$ with a sampling interval of 0.5km. The data are recorded by 247 receivers at the same depth with a sampling interval of 0.04km. As is commonly practiced, we perform the frequency continuation [Bunks et al., 1995] using three frequency bands of $\{2.0, 2.5, 3.0\}\text{Hz}$, $\{5.0, 6.0, 7.0\}\text{Hz}$, and $\{7.0, 8.0, 9.0\}\text{Hz}$. We discretize the model with 0.04km grids. We compare the performances of conventional FWI, conventional WRI, and the proposed LRWI. For conventional FWI and WRI, we use the l-BFGS method to solve the optimization problem, while we use Algorithm 1 to solve the LRWI. Due to the computational cost, we use LRWI to conduct an inversion on the lowest frequency band and then use the obtained model as the initial model for conventional FWI. All three approaches use 45 iterations for each frequency band.

To initialize the inversion, we conduct FWI and WRI with the 1D monotonously increasing velocity model $\mathbf{m}^{(0)}$ shown in Figure 1b. For LRWI we select $\theta^{(0)} = \frac{\pi}{4}$ and $\tilde{\mathbf{m}}^{(0)} = (\sin \theta^{(0)} \mathbf{m}^{(0)}, \cos \theta^{(0)} \mathbf{m}^{(0)})$. We conduct conventional WRI with four different selections of the penalty parameter λ , i.e. $\lambda = \beta_1 \mu_1 (\mathbf{A}^\top \mathbf{P}^\top \mathbf{P} \mathbf{A}^{-1})$ with $\beta_1 = 1e-8, 1e-4, 1e0$, and $1e4$. For the proposed LRWI, we use the same selection for λ and select six different γ 's for each λ . We select $\gamma = \beta_2 \mu_2 (\mathbf{T}(\lambda))$, with $\beta_2 = 1e-16, 1e-12, 1e-8, 1e-4, 1e0$, and $1e4$. The selections of β_1 and β_2 can not be extremely small, otherwise the matrix $\tilde{\mathbf{S}}(\beta_1, \beta_2)^\top \tilde{\mathbf{S}}(\beta_1, \beta_2)$ would be close to singular or badly scaled.

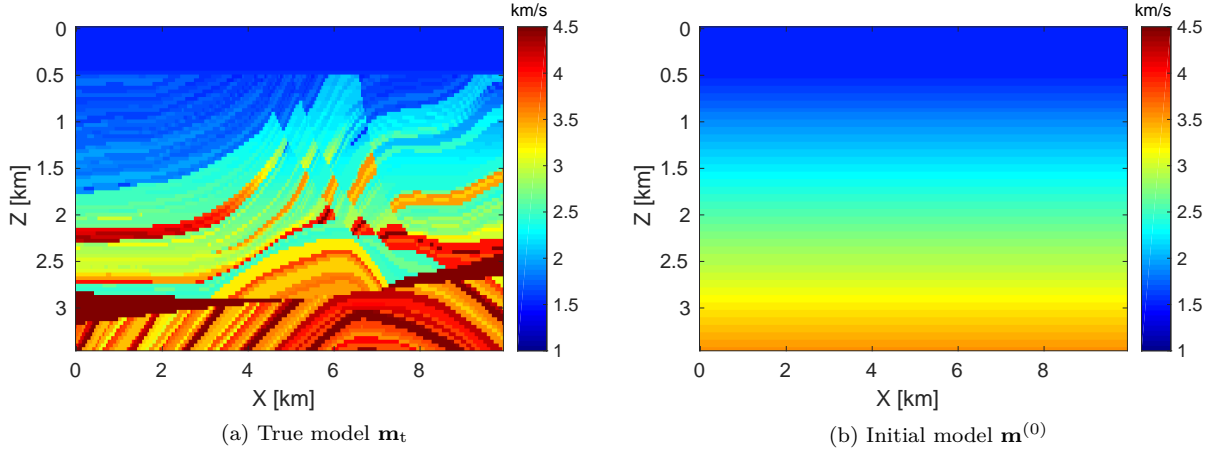


Figure 1: (a) The true velocity model; (b) The initial velocity model.

Before the inversion, we first study the condition number of the matrix $\tilde{\mathbf{S}}^\top \tilde{\mathbf{S}}$ with respect to the selection of β_1 and β_2 . We use the initial model $\mathbf{m}^{(0)}$ to form the Helmholtz matrix $\mathbf{A}(\mathbf{m}^{(0)})$ and compute the condition number of the matrix $\mathbf{A}(\mathbf{m}^{(0)})^\top \mathbf{A}(\mathbf{m}^{(0)})$ as a reference (c.f. the blue line in Figure 2). Then we use the initial model $\tilde{\mathbf{m}}^{(0)}$ and different selections of β_1 and β_2 to form the matrix $\tilde{\mathbf{S}}(\beta_1, \beta_2)^\top \tilde{\mathbf{S}}(\beta_1, \beta_2)$. The ranges for β_1 and β_2 are $[1e-3, 1e3]$ and $[1e-8, 1e4]$, respectively. The condition number of the matrix $\tilde{\mathbf{S}}(\beta_1, \beta_2)^\top \tilde{\mathbf{S}}(\beta_1, \beta_2)$ with respect to different selections of β_1 and β_2 are plotted in Figure 2. We can observe that when $1e-6 \leq \beta_2 \leq 1e0$, the condition number of $\tilde{\mathbf{S}}(\beta_1, \beta_2)^\top \tilde{\mathbf{S}}(\beta_1, \beta_2)$ is close to that of $\mathbf{A}(\mathbf{m}^{(0)})^\top \mathbf{A}(\mathbf{m}^{(0)})$. When $\beta_2 \leq 1e-6$, the condition number increases 10 times as β_2 decreases 100 times. When $\beta_2 \geq 1e0$, the condition number increases 10 times as β_2 increases 100 times. Compared to β_2 , β_1 possesses a less influence to the condition number of $\tilde{\mathbf{S}}(\beta_1, \beta_2)^\top \tilde{\mathbf{S}}(\beta_1, \beta_2)$. The variation of the condition number of $\tilde{\mathbf{S}}(\beta_1, \beta_2)^\top \tilde{\mathbf{S}}(\beta_1, \beta_2)$ with respect to β_1 is less than that of β_2 .

Figure 3 shows the relative model error $\frac{\|\mathbf{m}_t - \mathbf{m}_f\|_2}{\|\mathbf{m}_t\|_2}$ between the true model \mathbf{m}_t and the final inverted model \mathbf{m}_f obtained by conventional WRI and LRWI with different selections of β_1 and β_2 . According to Figure 3, the selection of $\beta_1 = 1e-4$ produces the best result for conventional WRI, and the selection of $\beta_1 = 1e-8$ and $\beta_2 = 1e-12$ produces the best result for the LRWI. Figure 4 shows the final inverted models \mathbf{m}_f of conventional FWI, WRI with the best selection of β_1 , and LRWI with the best selection of β_1 and β_2 . Figures 4a to 4c show the results of the three approaches using the data of the first frequency band. Clearly, under the current experimental settings, both FWI and WRI already converge to local minima at the first frequency band, despite the fact that WRI can outperform FWI in some other settings. On the other hand, LRWI provides a much better model for the following inversion, which yields a significantly better final result shown in Figure 4f compared to those obtained by FWI and WRI (c.f. Figures 4d and 4e).

Figure 3 does not include the result of LRWI with $\beta_2 = 1e-16$ due to the fact that the matrix $\tilde{\mathbf{S}}(\beta_1, \beta_2)^\top \tilde{\mathbf{S}}(\beta_1, \beta_2)$ is close to singular or badly scaled with such a small selection of β_2 . Therefore, we should avoid selecting too small β_2 when using LRWI. Figure 3 shows that with the selection of $\beta_1 \leq 1e0$ and $\beta_2 = 1e-12$ or

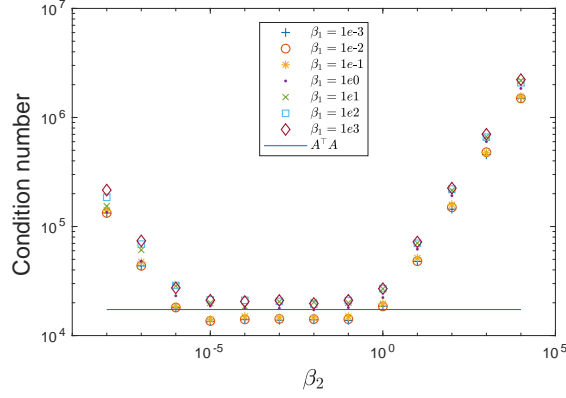


Figure 2: Condition number of the matrix $\tilde{\mathbf{S}}^T \tilde{\mathbf{S}}$ versus the values of β_1 and β_2 .

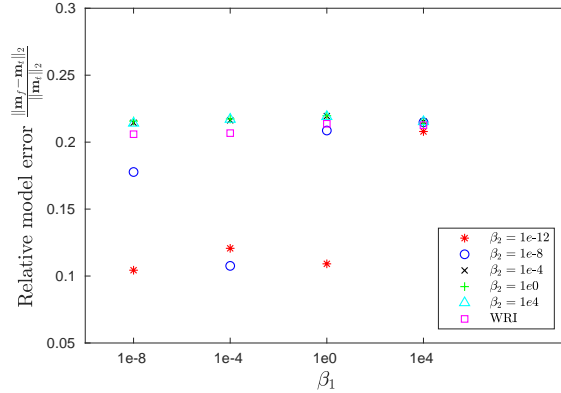


Figure 3: Relative model error comparison for WRI with different selections of β_1 and LRWI with different selections of β_1 and β_2 .

$\beta_1 = 1e-4$ and $\beta_2 = 1e-8$, LRWI can reconstruct an inverted model with a relative model error of 10%, which is significantly smaller than those of conventional WRI and LRWI with other selections of β_1 and β_2 . This result implies that when the initial model is poor, LRWI can bypass the local minima of conventional FWI and WRI by properly relaxing the wave-equation constraint and the rank-1 constraint.

To further compare the inverted results of the three approaches, we use the three inverted models shown in Figures 4a - 4c to compute the predicted data \mathbf{d}_{pred} at the frequency of 3 Hz for the source located at $x = 9$ km. We compute the absolute data differences $|\mathbf{d}_{\text{obs}} - \mathbf{d}_{\text{pred}}|$ between the observed data \mathbf{d}_{obs} and the predicted data \mathbf{d}_{pred} and depict them in Figure 5. The absolute data difference of FWI and WRI is more than 6 times larger than that of LRWI. This result coincides with the fact that FWI and WRI converge to local minima, while LRWI bypasses the local minima.

Robustness with respect to the starting frequency To investigate the robustness of the three methods with respect to the starting frequency, we conduct an additional experiment, in which we vary the starting frequency from 0.5 Hz to 3.0 Hz. We use the same initial model shown in Figure 1b. Figure 10 illustrates the relative model errors versus the starting frequency for all the three methods. According to the previous example, when the relative model error reaches around 18%, the inversion converges to a local minimum. The highest starting frequencies for conventional FWI, WRI, and LRWI to obtain an inverted model with an acceptable relative model error ($\leq 14\%$) are 1 Hz, 1 Hz, and 2 Hz, respectively. This comparison implies that

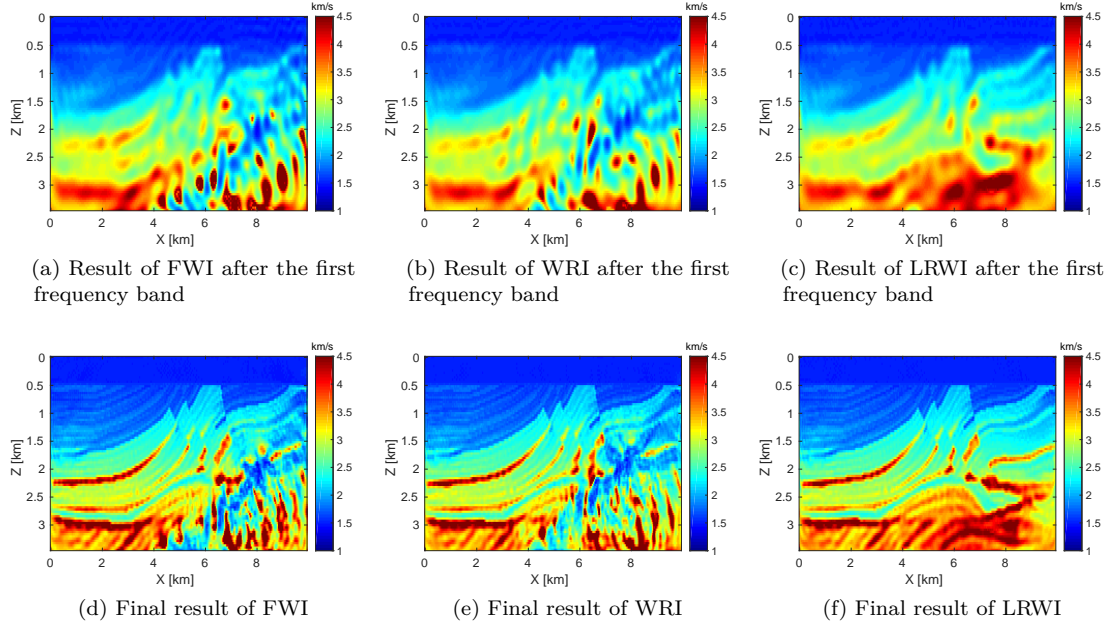


Figure 4: (a) - (c) Results of FWI, WRI, and LRWI after the first frequency band. (d) - (f) Final results of FWI, WRI, and LRWI.

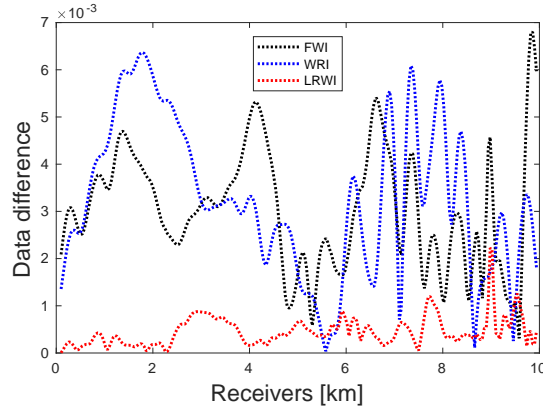


Figure 5: Comparison of the absolute data difference $|\mathbf{d}_{\text{obs}} - \mathbf{d}_{\text{pred}}|$ for the source located at $x = 9$ km and frequency of 3 Hz. The three lines denote the absolute data differences corresponding to the inverted results of FWI (black), WRI (blue), and LRWI (red) using the data of the the first frequency band.

under the aforementioned experimental settings, LRWI can conduct a successful inversion with a starting frequency twice large as that of conventional FWI and WRI.

Overthrust model

We conduct an experiment with the Overthrust model to investigate the generality of the proposed LRWI with respect to different velocity structures. Figure 7a shows the $5\text{km} \times 20\text{km}$ Overthrust model. We place

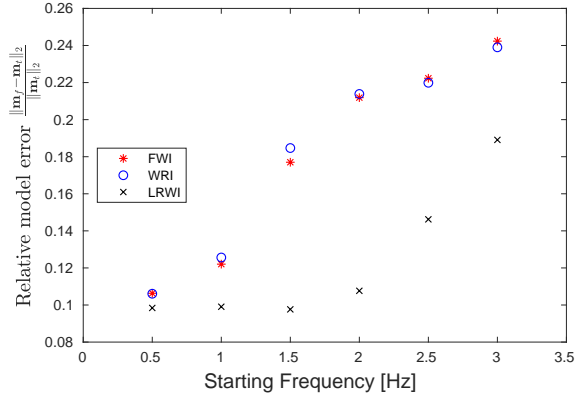


Figure 6: Relative model error comparison for FWI(*), WRI(\circ), and LRWI(\times) using data with different starting frequencies.

99 sources and 100 receivers at the depth of 0.1km with horizontal sampling intervals of 0.2km and 0.2km, respectively. As used in the example of the Marmousi model, we conduct the inversion with the frequency continuation strategy using three frequency bands of $\{2.0, 2.5, 3.0\}$ Hz, $\{5.0, 6.0, 7.0\}$ Hz, and $\{7.0, 8.0, 9.0\}$ Hz. We discretize the model with 0.05km grids. We use the same optimization strategy as that used in the Marmousi example for the inversion of conventional FWI, conventional WRI, and LRWI.

We conduct FWI and WRI with the initial model shown in Figure 7b. Similar to the previous example, we select $\theta^{(0)} = \frac{\pi}{4}$ and $\tilde{\mathbf{m}}^{(0)} = (\sin \theta^{(0)} \mathbf{m}^{(0)}, \cos \theta^{(0)} \mathbf{m}^{(0)})$ to initialize LRWI. We conduct conventional WRI with four different selections of the penalty parameter λ , i.e. $\lambda = \beta_1 \mu_1 (\mathbf{A}^\top \mathbf{P}^\top \mathbf{P} \mathbf{A}^{-1})$ with $\beta_1 = 1e-8, 1e-4, 1e0, \text{ and } 1e4$, and select the one that produces the result with the minimal relative model error as the output of WRI. For LRWI, we use the same selection for λ and select five different γ 's for each λ . We select $\gamma = \beta_2 \mu_2 (\mathbf{T}(\lambda))$, with $\beta_2 = 1e-16, 1e-12, 1e-6, 1e0, \text{ and } 1e6$. The combination of β_1 and β_2 that produces the result with the minimal relative model error is selected as the output of LRWI.

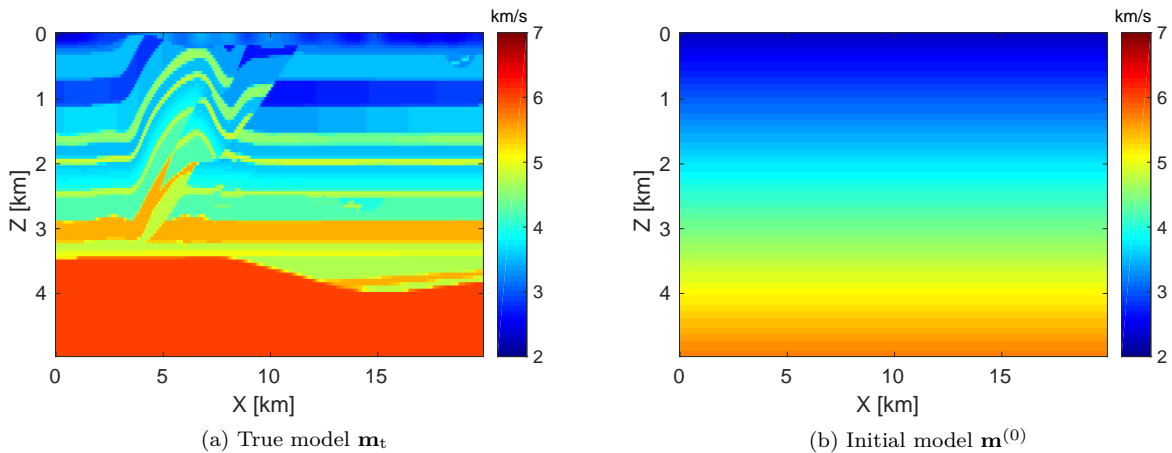


Figure 7: (a) The true velocity model; (b) The initial velocity model.

Figure 8 shows the comparison of the final relative model errors for results obtained by conventional WRI using different β_1 and LRWI using different β_1 and β_2 . We did not include the result of LRWI with $\beta_2 = 1e-16$,

since the matrix $\tilde{\mathbf{S}}(\beta_1, \beta_2)^\top \tilde{\mathbf{S}}(\beta_1, \beta_2)$ is close to singular or badly scaled. According to Figure 8, the selection of $\beta_1 = 1e-4$ produces the best result for WRI, and the selection of $\beta_1 = 1e-8$ and $\beta_2 = 1e-12$ produces the best result for LRWI. Figure 9 shows the results of FWI, WRI with the best selection of β_1 , and LRWI with the best selection of β_1 and β_2 . Figures 9a to 9c show the results of the three approaches using the data of the first frequency band, and Figures 9d to 9f show the final results of the three approaches. Clearly, at the first frequency band, FWI and WRI already converge to the local minima, while LRWI provides a much better model for the following inversion, which yields a final result (c.f. Figure 9f) that has the minimal relative model error and matches the true model significantly better than those obtained by FWI and WRI (c.f. Figures 9d and 9e).

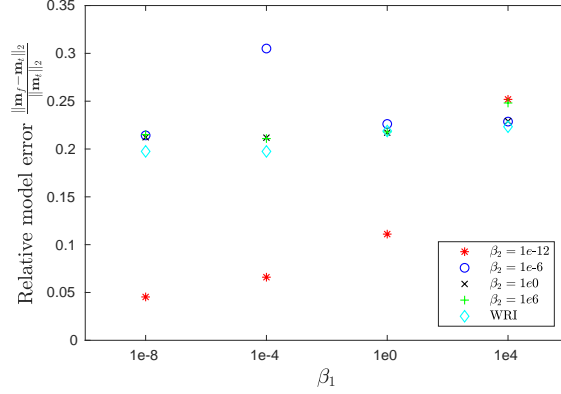


Figure 8: Final model error comparison for WRI with different selections of β_1 and rank-2 WRI with different selections of β_1 and β_2 .

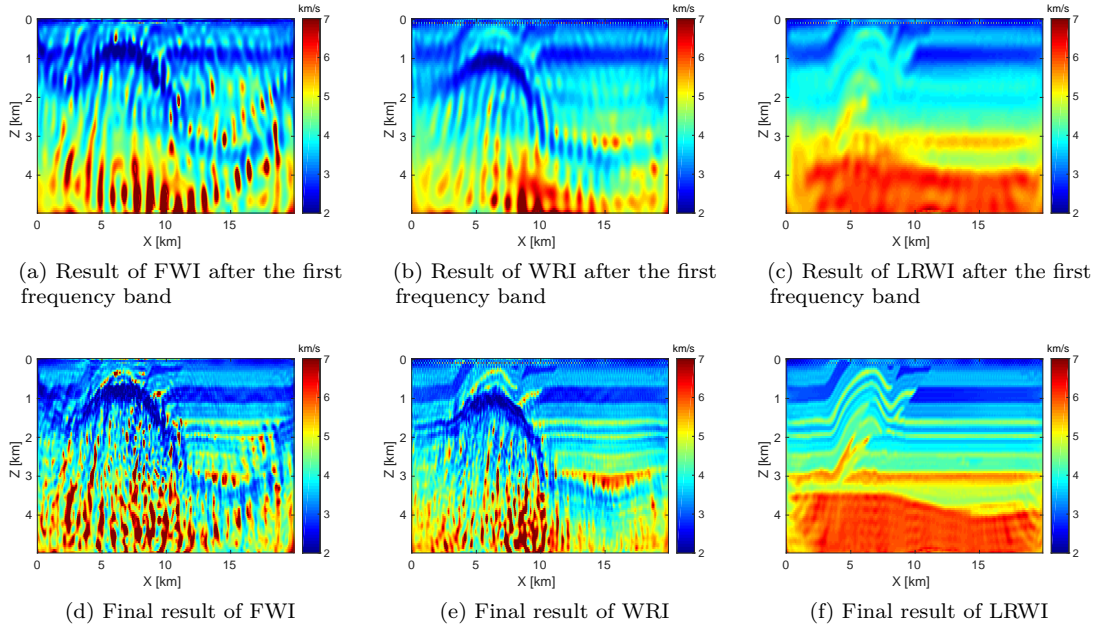


Figure 9: (a) - (c) Results of FWI, WRI, and LRWI after the first frequency band. (d) - (f) Final results of FWI, WRI, and LRWI.

Figure 8 shows that LRWI obtains inverted models with relative model errors less than 10% with the selection of $(\beta_1, \beta_2) = (1e-4, 1e-12)$ and $(1e-8, 1e-12)$, while the relative model errors for results of WRI are larger than 20%. This comparison illustrates that LRWI with an appropriate relaxation on the rank-1 constraint and the PDE constraint can mitigate the local minima of FWI and WRI.

Robustness with respect to the starting frequency We also conduct an example to investigate the robustness of the three methods with respect to the starting frequency for the Overthrust model. In this example, we vary the starting frequency from 0.5 Hz to 3.0 Hz. We use the same initial model shown in Figure 7b. Figure 10 illustrates the relative model errors versus the starting frequency for all the three methods. The highest starting frequencies for FWI, WRI, and LRWI to obtain an inverted result with an acceptable relative model error ($\leq 10\%$) are 0.5 Hz, 0.5 Hz, and 2.5 Hz, respectively. This comparison implies that under the aforementioned experimental settings, LRWI can conduct a successful inversion with a starting frequency fifth large as that of conventional FWI and WRI.

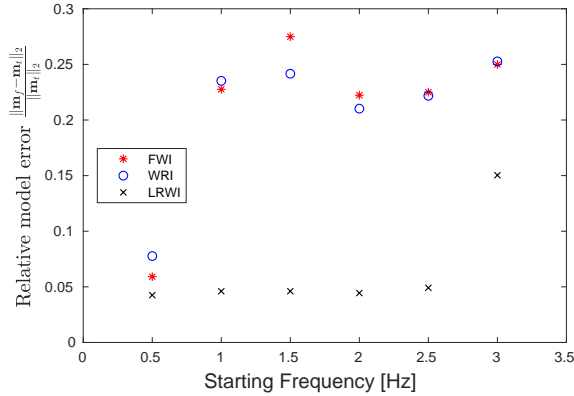


Figure 10: Relative model error comparison for FWI(*), WRI(o), and LRWI(x) using data with different starting frequencies.

Discussions

This paper introduces the basics of a “Lift” and “Relax” approach for the waveform inversion with PDE constraints. We have presented promising initial results in mitigating problems of local minima, while some aspects of the proposed approach warrant further investigations.

The selection of the penalty parameters λ and γ are essential to the success of the proposed LRWI as shown in both numerical examples. While our analysis and results imply that selecting λ to be a small fraction of the largest eigenvalue of $\mathbf{A}^\top \mathbf{P}^\top \mathbf{P} \mathbf{A}^{-1}$ and selecting γ to be a small fraction of the largest fraction between the ℓ_2 -norms of the vectors $\text{diag}(\mathbf{T}_{i,j}(\lambda))$ and $\hat{\mathbf{m}}_i \odot \hat{\mathbf{m}}_j$ at initial iterations yields plausible results, a more solid justification of this observation would be desirable for more robust approaches.

While we can use LRWI to conduct inversion with low-frequency data and produce a good initial model for conventional FWI with a small computational cost, the application of the LRWI to high-frequency data can further help us bypass more potential local minima in the objective function of conventional FWI. To address high-frequency data, a fast solver for Equation 15 would be worthwhile. One possible solution is to use efficient direct or iterative solvers designed for the Helmholtz equation as a preconditioner for the linear system in Equation 15.

Finally, the rank of the lifted matrices could be potentially worth exploring. In this work, we lift the unknown variables from vectors to rank-2 matrices due to the consideration of storage and computational cost. Indeed,

if the storage and computational cost are not bottlenecks, we can lift the unknown variables to matrices with higher ranks and study the effect of the rank on the final inversion results.

Conclusions

We have presented a “Lift” and “Relax” approach for waveform inversion problems with PDE constraints. The proposed method is based on a PDE relaxation and a rank-2 variable relaxation. The reformulation results in an unconstrained optimization problem with respect to a rank-2 matrix that contains both lifted model parameters and wavefields. To avoid storing and updating the rank-2 wavefields during the optimization, we use the variable projection method to explicitly eliminate the rank-2 wavefields by solving an overdetermined linear system. We show that the proposed approach is able to explore a much larger search space with an acceptable additional computational cost compared to conventional FWI and WRI.

The main algorithmic difference with conventional FWI and WRI is the rank-2 variable lifting and the resulting overdetermined system required to solve. Instead of solving PDEs, we formulate an overdetermined system of equations that consists of the discretized rank-2 PDE, the measurements, and the rank-1 regularizations. We study the properties of this overdetermined system with respect to the selection of the penalty parameters λ and γ . We show that the condition number of the overdetermined system can reach a similar value as that of the original PDE by tuning the two parameters. Therefore, it is plausible that we can solve the overdetermined system as efficiently using a similar approach as is applied to the original PDE.

The numerical examples show that the proposed LRWI is able to conduct successful inversion with higher-frequency data and poorer initial models compared with conventional FWI and WRI. The numerical examples further show that through tuning the penalty parameters λ and γ , the proposed approach can find a search path in the enlarged space that bypasses the potential local minima in the objective function of conventional FWI and WRI.

Acknowledgments

The authors acknowledge the funding and support provided by ExxonMobil Research and Engineering Company. Dr. Laurent Demanet is also supported by AFOSR grant FA9550-17-1-0316.

References

- F Aminzadeh, N Burkhard, J Long, T Kunz, and P Duclos. Three dimensional seg/eage models - an update. *The Leading Edge*, 15:2, 1996.
- Carey Bunks, Fatimetou M Saleck, S Zaleski, and G Chavent. Multiscale seismic waveform inversion. *Geophysics*, 60(5):1457–1473, 1995.
- M Cara and JJ L ev eque. Waveform inversion using secondary observables. *Geophysical Research Letters*, 14(10):1046–1049, 1987.
- Augustin Cosse, Stephen D Shank, and Laurent Demanet. A short note on rank-2 relaxation for waveform inversion. In *SEG Technical Program Expanded Abstracts 2015*, pages 1344–1350. Society of Exploration Geophysicists, 2015.
- Bjorn Engquist and Brittany D Froese. Application of the Wasserstein metric to seismic signals. *Communications in Mathematical Sciences*, 12:979–988, 2014.

- Zhilong Fang, Curt Da Silva, Rachel Kuske, and Felix J Herrmann. Uncertainty quantification for inverse problems with weak partial-differential-equation constraints. *Geophysics*, 83(6):R629–R647, 2018a.
- Zhilong Fang, Rongrong Wang, and Felix J Herrmann. Source estimation for wavefield-reconstruction inversion. *Geophysics*, 83(4):R345–R359, 2018b.
- Gene Golub and Victor Pereyra. Separable nonlinear least squares: the variable projection method and its applications. *Inverse Problems*, 19(2):R1, 2003.
- Guanghai Huang, Rami Nammour, and William Symes. Full-waveform inversion via source-receiver extension. *Geophysics*, 82(3)(3):R153–R171, 2017.
- Jean B Lasserre. Global optimization with polynomials and the problem of moments. *SIAM Journal on optimization*, 11(3):796–817, 2001.
- Monique Laurent. Sums of squares, moment matrices and optimization over polynomials. In *Emerging applications of algebraic geometry*, pages 157–270. Springer, 2009.
- Yunyue Li, Biondo Biondi, Robert Clapp, and Dave Nichols. Wave-equation migration velocity analysis for vti models. *Geophysics*, 79(3):WA59–WA68, 2014.
- Jorge Nocedal and Stephen J Wright. *Numerical Optimization*. Springer-Verlag New York, 2006. doi: 10.1007/978-0-387-40065-5.
- R Gerhard Pratt. Seismic waveform inversion in the frequency domain, Part 1: Theory and verification in a physical scale model. *Geophysics*, 64(3):888–901, 1999.
- William W Symes. Migration velocity analysis and waveform inversion. *Geophysical prospecting*, 56(6): 765–790, 2008.
- Albert Tarantola and Bernard Valette. Generalized nonlinear inverse problems solved using the least squares criterion. *Reviews of Geophysics*, 20(2):219–232, 1982. ISSN 1944-9208. doi: 10.1029/RG020i002p00219. URL <http://dx.doi.org/10.1029/RG020i002p00219>.
- Tristan van Leeuwen and Felix J. Herrmann. A penalty method for PDE-constrained optimization in inverse problems. *Inverse Problems*, 32(1):015007, 12 2015. URL <https://www.slim.eos.ubc.ca/Publications/Public/Journals/InverseProblems/2015/vanleeuwen2015IPpmp/vanleeuwen2015IPpmp.pdf>.
- Tristan van Leeuwen and WA Mulder. A correlation-based misfit criterion for wave-equation traveltime tomography. *Geophysical Journal International*, 182(3):1383–1394, 2010.
- Roelof Versteeg. The marmousi experience: Velocity model determination on a synthetic complex data set. *The Leading Edge*, 13(9):927–936, 1994.
- DV Vigh, WES Starr, and KD Kenneth Dingwall. 3d prestack time domain full waveform inversion. In *71st EAGE Conference and Exhibition incorporating SPE EUROPEC 2009*, 2009.
- Jean Virieux and Stéphane Operto. An overview of full-waveform inversion in exploration geophysics. *Geophysics*, 74(6)(6):WCC1–WCC26, 2009. doi: 10.1190/1.3238367. URL <http://dx.doi.org/10.1190/1.3238367>.
- Michael Warner and Lluís Guasch. Adaptive waveform inversion: Theory. *Geophysics*, 81(6)(6):R429–R445, 2016.
- Mike Warner, Tenice Nangoo, Nikhil Shah, Adrian Umpleby, Joanna Morgan, et al. Full-waveform inversion of cycle-skipped seismic data by frequency down-shifting. In *83th Annual International Meeting*, pages 903–907. SEG, Expanded Abstracts, 2013.

Ru-Shan Wu, Jingrui Luo, and Bangyu Wu. Ultra-low-frequency information in seismic data and envelope inversion. In *SEG Technical Program Expanded Abstracts 2013*, pages 3078–3082. Society of Exploration Geophysicists, 2013.

Yunan Yang, Björn Engquist, Junzhe Sun, and Brittany F Hamfeldt. Application of optimal transport and the quadratic wasserstein metric to full-waveform inversion. *Geophysics*, 83(1)(1):R43–R62, 2018.